Liquid gallium cooling of silicon crystals in high intensity photon beams (invited)

R. K. Smither and G. A. Forster

Argonne National Laboratory, Argonne, Illinois 60439

D. H. Bilderback, M. Bedzyk, K. Finkelstein, C. Henderson, and J. White

Cornell University, Ithaca, New York 14853

L. E. Berman, P. Stefan, and T. Oversluizen

Brookhaven National Laboratory, Upton, New York 11973

(Presented on 31 August 1988)

The high-brilliance, insertion-device-based photon beams of the next generation of synchrotron sources (Argonne's APS and Grenoble's ESRF) will deliver large thermal loads (1–10 kW) to the first optical elements. Considering the problems that present synchrotron users are experiencing with beams from recently installed insertion devices, new and improved methods of cooling these first optical elements, particularly when they are diffraction crystals, are clearly needed. A series of finite element calculations were performed to test the efficiency of new cooling geometries and various cooling fluids. The best results were obtained with liquid Ga metal flowing in channels just below the surface of the crystal. Ga was selected because of its good thermal conductivity and thermal capacity, low melting point, high boiling point, low kinetic viscosity, and very low vapor pressure. Its very low vapor pressure, even at elevated temperatures, makes it especially attractive in UHV conditions. A series of experiments were conducted at CHESS in February of 1988 that compared liquid gallium-cooled silicon diffraction crystals with water-cooled crystals. A six-pole wiggler beam was used to perform these tests on three different Si crystals, two with new cooling geometries and the one presently in use. A special high-pressure electromagnetic induction pump, recently developed at Argonne, was used to circulate the liquid gallium through the silicon crystals. In all experiments, the specially cooled crystal was used as the first crystal in a two crystal monochromator. An infrared camera was used to monitor the thermal profiles and correlated them with rocking curve measurements. A second set of cooling experiments were conducted in June of 1988 that used the intense, highly collimated beam from the newly installed ANL/CHESS undulator. Tests were performed on two new Ga-cooled Si crystals and compared with the standard water-cooled Si crystal. One of the crystals had cooling channels at two levels in the crystal that allowed one to actively control the shape of the crystal surface. The second one had rectangular cooling channels located just beneath the diffraction surface. Both crystals showed major improvements over the water-cooled crystal.

INTRODUCTION

The high-brilliance, insertion-device-based x-ray beams of the next generation of synchrotron sources, Argonne's APS, Grenoble's ESRF, and Japan's PF, will deliver large thermal loads to various components in the beamlines. The first optical element will often absorb the full heat of these intense x-ray beams which will range in power from 1 to 20 kW. The increased collimation of the next generation sources will increase the seriousness of these problems still further. Hence, improved methods of cooling the first optical elements, particularly when they are diffraction crystals, are clearly needed.

Liquid metal cooling has worked well in other high heat load applications, particularly in high-temperature reactors, and appeared to be a good solution in this case as well. After consulting the large bank of information on liquid metals available at ANL, liquid gallium was chosen as the most promising cooling fluid.[1] Liquid gallium has good thermal conductivity and thermal capacity, a low melting point, and a high boiling point. Its very low vapor pressure, even at elevated temperatures, makes it especially attractive in UHV conditions.

I. PRESENT COOLING PROBLEMS

An example of the heat load problems encountered at operating synchrotron facilities is the two crystal monochromator used on the A2 beamline at CHESS. This monochromator intercepts one third of the beam (640 W for 70 mA running at 5.4 GeV) from the six-pole electromagnetic wiggler. The output of this monochromator increased with increasing beam current until the current approached 10 mA and then leveled off giving no further improvement as the beam current was increased to 70 mA. Thus a factor of 7 in intensity was lost due to the distortion of the crystal by the heat load. When this problem was analyzed in detail it was found that the distortion of the first crystal spreads out the diffracted beam in both angle and energy so that only some of the x rays have the right incident angle and energy to be diffracted by the second crystal of the monochromator. The observed rocking curves, taken by rotating the second crys-

 0034-6748/89/071486-07$01.30

tal, are given in Fig. 1. The different curves are labeled with the corresponding current (electrons) in the storage ring. High temperatures and large distortions occur at small values of the ring current because of the long path that the heat must travel to exit the crystal.

II. SURFACE TEMPERATURES AND CRYSTAL DISTORTIONS

The temperature of the surface of the diffraction crystal (T_1) relative to the initial temperature of the cooling fluid (T_f) is given by Eq. (1):

$$T_1 = \Delta T_{12} + \Delta T_{23} + \Delta T_3 + T_f, \tag{1}$$

where ΔT_{12} is the temperature difference across the crystal, ΔT_{23} is the temperature difference between the crystal surface adjacent to the cooling fluid and the cooling fluid, and ΔT_3 is the change in temperature of the cooling fluid relative to its initial input temperature, T_f.

These temperature distributions generate three different kinds of distortions in the diffraction crystal. The first two are illustrated in Fig. 2. First, there is the overall bending or bowing of the crystal caused by the thermal gradients in the crystal, second, there is the thermal bump (shaded area) that is caused by the expansion of the crystal perpendicular to the surface and third, there is the change in the crystal lattice spacing through thermal expansion caused by the increase in the surface temperature of the crystal. These effects vary over the surface of the crystal, following the variation in thermal loading of the surface. In the case of a crystal of uniform thickness, heated uniformly on the top surface and cooled uniformly on the bottom surface, the bowing of the surface is given by Eqs. (2)–(4):

$$R = D/\alpha\,\Delta T_{12} = k/\alpha Q, \tag{2}$$

$$\Delta T_{12} = T_1 - T_2 = QD/k, \tag{3}$$

$$\Delta\Theta_b = \Delta x\, k/\alpha Q, \tag{4}$$

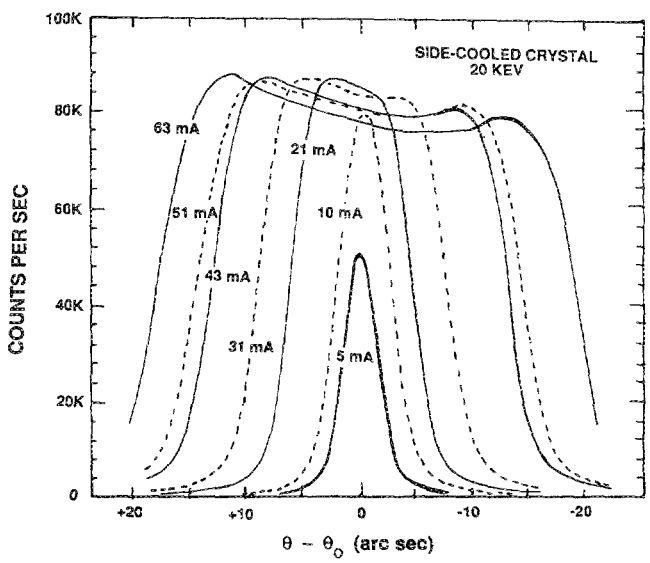

FIG. 1. Comparison of the rocking curves for the second crystal in the two-crystal monochromator when the first crystal in the monochromator is the standard CHESS side-cooled crystal, for different electron beam currents in the storage ring.

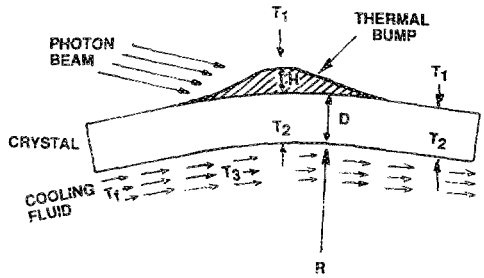

FIG. 2. Schematic drawing of the different thermal distortions of a diffraction crystal subject to high heat loads from synchrotron beams.

where D is the thickness of the crystal, R is the radius of curvature of the crystal generated by Q, the heat load per unit area, α is the thermal coefficient of expansion, k is the thermal conductivity, ΔT_{12} is the temperature difference between the top (T_1) and bottom surface (T_2), and $\Delta\Theta_b$ is the change in angle or angular error that occurs as one moves a distance Δx along the surface of the bowed crystal. The value of R is independent of the thickness of the crystal D and depends only on the parameters, k and α, of the crystal material and the heat flow, Q, through the crystal. If ΔT_{12} is 50 °C and D is 1.5 cm and α is 3×10^{-6} °C (for silicon), then $R = 100$ m. This corresponds to heat flow through the crystal of $Q = 50$ W per cm^2, from Eq. (2), where $k = 1.5$ W per cm per °C (for silicon). In this example a distance of 1 cm along the face of the bowed crystal corresponds to a change in angle, and thus an angular error, of 20.4 arcsec.

If heat is added nonuniformly to the front face of the crystal, varying from zero to Q at the center of the beam, then the height (H) of the thermal bump is given to first order by Eq. (5):

$$H = \alpha\,\Delta T_{12}\,D/2 \cong \alpha Q D^2/2k, \tag{5}$$

where Q is now the heat load at the center of the thermal bump. Note that the value of H is proportional to D^2 and thus very sensitive to the thickness of the crystal. If the shape of the thermal bump is Gaussian with a FWHM of $2X$, then the maximum slope and thus maximum angular error, $\Delta\Theta_{\max}$, is given by Eq. (6):

$$\Delta\Theta_{\max} = 1.43(H/2X) = 1.43(H/\mathrm{FWHM}). \tag{6}$$

Using the above parameters and a $2X = 2$ cm, $\Delta\Theta_{\max} = 16.4$ arcsec. This is similar to the angular error $\Delta\Theta_b = 20.4$ arcsec obtained by moving 1 cm along the surface of the bowed crystal mentioned above. This thermal-bump angular error increases the incident angle of the photon beam on the upstream side of the thermal bump and decreases it on the down side of the bump, giving a maximum spread of angular errors of 32.8 arcsec.

The third type of distortion produced by the photon beam is the change in the spacing between crystalline planes with the increase in the surface temperature of the crystal. For a given wavelength this change in spacing is equivalent to a change in the diffraction angle, $\Delta\Theta_d$, which is given by Eq. (7):

$$\Delta\Theta_d = -\alpha\,\Delta T \tan\Theta \cong -\alpha\,\Delta T\,\Theta, \tag{7}$$

where ΔT is the variation in the temperature of the crystal

surface. A 50 °C temperature rise will change the lattice spacing by $\alpha\,\Delta T = 1.5\times10^{-4}$ and give an equivalent angular error of $\Delta\Theta_d = 3.0$ arcsec for a 20-keV photon beam diffracted by (111) Si planes and $\Delta\Theta_d = 7.5$ arcsec for an 8-keV photon beam. The d spacing errors, $\Delta\Theta_d$ are all in one direction so they cause an asymmetry in the overall angular error relative to the center of the photon beam. The $\Delta\Theta_d$ errors are 5–10 times less than the other two mentioned above and are comparable to the Darwin widths for these cases so they result in only a modest increase in the angular errors. These estimates of the relative importance of the different distortions are in agreement with the calculations of Edwards *et al.*[2]

III. HEAT TRANSFER TO THE COOLING FLUID

The temperature difference, ΔT_{13}, between the surface of the crystal and the cooling fluid (see Fig. 2) is made up of two parts as shown in Eq. (8):

$$\Delta T_{13} = \Delta T_{12} + \Delta T_{23}. \tag{8}$$

The first part, ΔT_{12}, is the same temperature difference that was discussed above and corresponds to the temperature difference across the crystal in Fig. 2. The second part, ΔT_{23}, is the temperature difference between the inner wall of the crystal (T_2) and the cooling fluid (T_3). This is given by Eqs. (9) and (10)[3]:

$$\Delta T_{23} = Q/h, \tag{9}$$

$$h = A_1 k/d + A_2(k^{0.6}C_v^{0.4}/d^{0.2}\nu^{0.8})V^{0.8}, \tag{10}$$

where Q is the heat load per unit area and h is the heat transfer coefficient at the solid-liquid interface. h consists of two parts, the first of which involves the thermal conductivity k divided by d, the effective hydraulic diameter, which reflects the size and shape of the cooling channels. The second term includes the ratio of k and d and in addition, C_v is the specific heat per unit volume, V is the velocity, and ν is the kinetic viscosity of the cooling fluid. A_1 and A_2 are constants. The second term contains the velocity of the cooling fluid and therefore, becomes the dominant term at high flow rates while the first term dominates at low flow rates.

IV. CHOICE OF GALLIUM AS THE COOLING FLUID

The finite element analysis[1] was also used to compare different cooling fluids[1] and made it quite clear that liquid metals were more efficient cooling fluids than water under almost all conditions. Ga was the most attractive of the liquid metals for synchrotron applications.[1] Table I compares the physical properties of liquid gallium with water. These physical properties directly effect the value of h used to calculate ΔT_{23} in Eqs. (9) and (10). The biggest difference between the two cooling fluids comes in the values for k, their thermal conductivity. The high value of k for gallium makes both terms in Eq. (10) important while the very low value of k for water makes the first term very small and the second term small as well until the fluid velocity (V) becomes large. A plot of h verses flow rates for liquid gallium (upper curve) and water (lower curve) in 0.5-cm-diam channels, is given in Fig. 3. One can see immediately from this plot why gallium is the preferred cooling fluid. The value of h for gallium starts out much higher than that for water because of gallium's much larger thermal conductivity (k) and remains higher at all flow rates because the coefficient on the second term is also larger for gallium than for water.

TABLE I. Comparison of fluid properties of Ga and H_2O. Figure of merit $= C_v x k$.

	Gallium	H_2O
Density (g/cc) (40 °C)	6.1	1.0
Melting point (°C)	29.8	0.0
Boiling point (°C)	2205.0	100.0
Vapor pressure (mm/Hg) (100 °C)	10^{-10}	760.0
Thermal conductivity (W/cm,°C)	0.41	0.0068
Vol. heat capacity (Joules/cc,°C)	2.2	4.2
Viscosity (cp) (40 °C)	1.6	1.0
Kinetic viscosity (cp/g/cc)	0.27	4.2
Figure of merit (Vol. heat cap. × thermal cond.)	0.90	0.029

V. ELECTROMAGNETIC INDUCTION PUMP

The liquid gallium is pumped through channels just below the surface of the silicon crystal with an electromagnetic induction pump developed at the Argonne National Laboratory for this purpose.[1] The interaction of the moving magnetic field and the current generates a continuous, nonpulsating force on the liquid gallium that produces the pumping action. The pump develops a static head pressure of 45 psi and can pump up to 3 gpm through a typical cooling system with a silicon crystal mounted a few feet away from the pump. The essential features and the new developments in this pump are its high head pressure and its smooth, nonpulsating flow. Most liquid metal pumps are low pressure devices. The high pressure is needed to push the liquid gallium through the crystal cooling system at the high flow rates (1–3 gpm) needed to obtain optimum cooling of the crystals.

VI. COOLING EXPERIMENTS WITH WIGGLER BEAMS

Water is used as the cooling fluid in most present day synchrotron facilities but as mentioned above, is not efficient

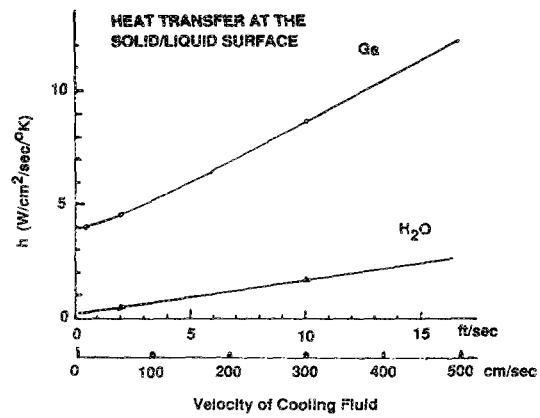

FIG. 3. Plot of h, the transfer coefficient, for liquid Ga (upper curve) and for water (lower curve) as a function of cooling fluid flow rate in a 0.5-cm-diam channel.

enough to cool some of the more recently developed beams for newly installed wigglers and undulators and will encounter even more difficulties when trying to cool the insertion device beams at the next generation of synchrotrons (APS, ESRF, etc.).[1] This makes it very important to start investigating new cooling fluids and new cooling geometries.

A set of experiments were performed in February 1988, using the radiation from the six-pole wiggler at CHESS. A comparison was made between the performance of three silicon crystals as x-ray monochromators cooled with either liquid gallium or water. The two gallium-cooled Si crystals had 5-mm-diam cooling channels drilled through them just below the diffraction surface (111). One crystal measured 7.5×7.5 cm^2 (diffraction area) by 1.5 cm thick and had five cooling channels whose center lines were 5 mm below the surface. The second channel-cooled crystal was 10 cm long in the direction of the beam, 3.8 cm wide and 2.5 cm thick, with three 5-mm-diam cooling channels with centers 5 mm below the surface. The third crystal used in these tests was the Si crystal that is normally used in the CHESS monochromator on beamline A2. This crystal has the same dimensions as the crystal with three cooling channels described above but was cooled on three sides with water-cooled copper blocks thermally coupled to the crystal through an indium-gallium eutectic interface. Tests were also run on the three-channel crystal with water cooling. The cross sections of these three crystals is shown in Fig. 4.

In all tests, the specially cooled crystal was used as the first crystal in a two crystal monochromator and received the full power (640 W for 70 mA running at 5.4 GeV) from the wiggler source. The wiggler is 14.5 m from the first crystal in the double-crystal monochromator. The second crystal, located a few centimeters downstream, diffracts the beam a second time, returning it to the horizontal direction. The doubly diffracted beam is then analyzed in a hutch located 7.5 m farther downstream. An infrared camera was used to monitor the thermal profile of the photon beam on the crystals. This made it possible to measure the height and shape of the thermal profile with different stored ring currents in the synchrotron and when carbon absorbers of different thickness were placed in the photon beam. Figure 5 shows the thermal profile obtained with the three different crystals with 46 mA in the storage ring and compares the thermal profiles of one of the crystals when cooled with either gallium or water. The highest profile is that for the standard CHESS crystal with side cooling. The next three are for the three-channel crystal. Water was used as the cooling fluid for the higher of the three and gallium for the next lower two. The lowest thermal profile is for the five-channel crystal with gallium cooling. The improved cooling of this last case comes from a better cooling geometry. The infrared measurements were correlated with rocking curve measurements at 8 and 20 keV, made by rotating the second crystal in the monochromator and with scanning slit measurements of the beam profile. At low-photon beam intensities corresponding to low-electron beam currents in the storage ring, almost all of the photons that are diffracted by the first crystal are also diffracted by the second crystal.

A comparison of the rocking curves obtained for the different crystals with different cooling fluids is shown in Fig. 6. The lower dashed curve corresponds to the standard CHESS side-cooled crystal that was discussed in Sec. I. The use of water cooling near the surface, in the three-channel crystal, reduced the distortion in the crystal by about 36% (when compared with the side-cooled crystal), with a corresponding increase in the peak intensity. This case is shown in Fig. 6 as the higher dashed curve. When Ga was used for the cooling fluid in this crystal, the rocking curve becomes narrower and higher (lower solid line). When the Ga flow rate in the crystal was increased to 1.33 gpm, the distortion was reduced by another 30%. The best results were obtained with the Ga-cooled five-channel crystal (upper solid curve) which increased the peak intensity by a factor of 3–5 (depending on the energy and cooling fluid flow rate) over that

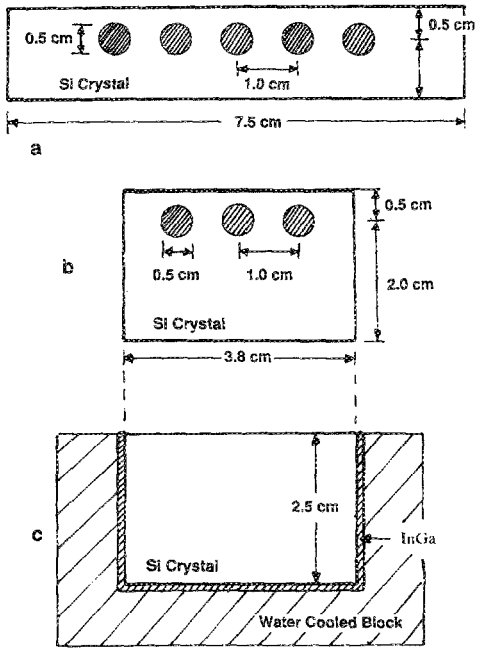

FIG. 4. Drawings of the cross sections of the three cooled silicon crystals used in the wiggler experiments.

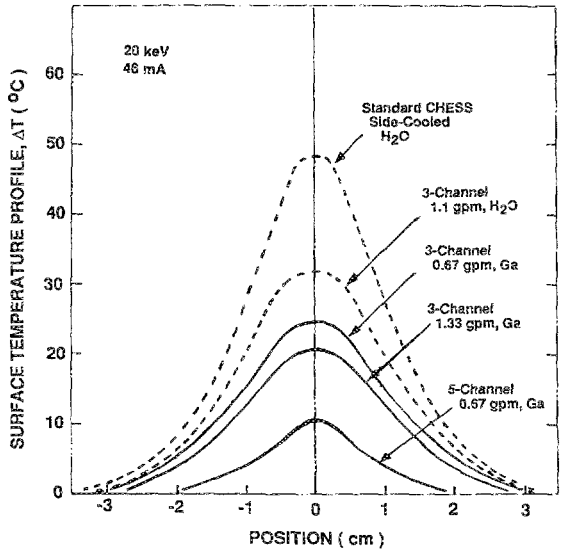

FIG. 5. Plot of the surface temperature profile in the direction of the beam for the three different cooled silicon crystals used in the wiggler experiments.

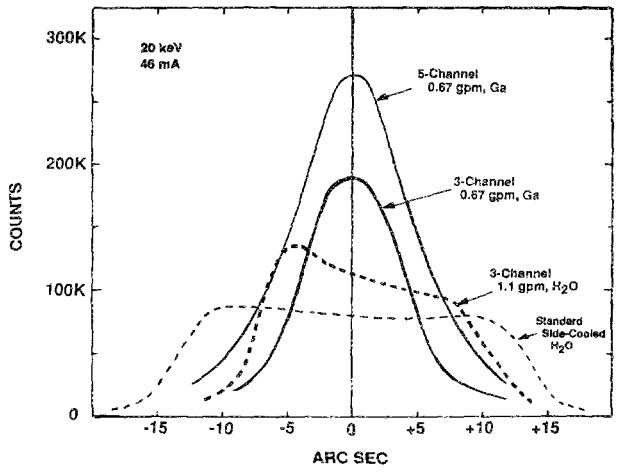

FIG. 6. Plot of the rocking curves obtained with the three different silicon crystals in the wiggler experiments (photon energy of 20 keV, electron current of 46 mA).

obtained with the side-cooled crystal. Figure 7 shows the rocking curve for the five-channel crystal when different carbon absorbers were put into the photon beam. The observed intensity with the full beam (46 mA) is 5% less the predicted value, so the loss of intensity with the full beam is almost within our experimental error. This suggests that the intensity of the beam could be appreciably higher before major distortion occurs that would limit the intensity of the beam diffracted by the second crystal. The five-channel crystal is known to have a small mosaic structure and this may account for some of its better diffraction efficiency and lower sensitivity to thermal loads. A detailed analysis of the thermal profiles observed for the five-channel crystal and comparison with the calculated results suggests that the channels could be closer to the surface by a factor of 2.5 if the channels were made smaller. This would reduce the height of the thermal profile and the amount of distortion of the crystal surface by a similar factor of 2.5 for the bowing errors and a factor of 6.25 for the thermal bump errors. This would allow one to increase the intensity of the primary beam by a similar factor of 2.5 without serious losses in the final diffracted beam intensity.

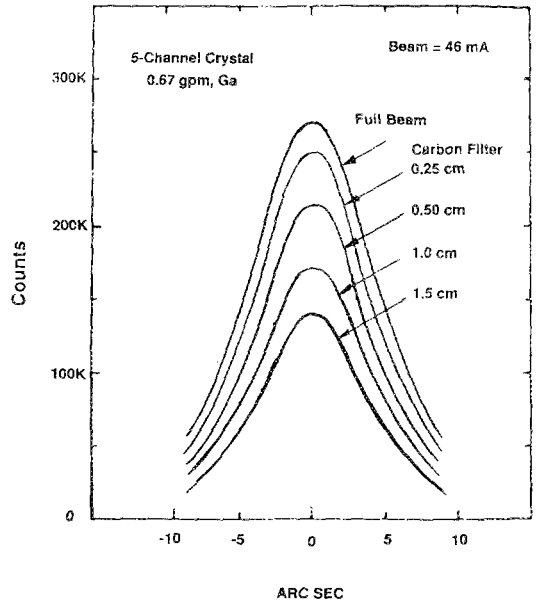

FIG. 7. Plots of rocking curves for the five channel crystal for different thicknesses of the stepped carbon filter in the photon beam.

VII. COOLING EXPERIMENTS WITH UNDULATOR BEAMS

A second set of experiments were performed at CHESS in June of 1988. They used the intense photon beams generated by the newly installed ANL/CHESS undulator.[4,5] The experimental setup was the same as that used in the previous cooling experiments except that the distance from the undulator to the first crystal was 18.5 m and the detector station located 7.5 m farther down stream. As before, an electromagnetic induction pump was used to circulate liquid gallium through channels in the first crystal. Two new silicon crystals with new cooling geometries were tested and compared to the performance of the side-cooled crystal. The cross section and thermal footprint of one of these new crystals is shown in Fig. 8. It has a very thin top layer, 0.76 mm, cooled by slots 2.33 mm wide and supported by fins or ribs 0.80 mm wide. This upper structure was fabricated as a single piece and cemented to a 19-mm-thick base crystal.[6] It was designed to test the dependence of the crystal distortions on the thickness of the top layer [see Eqs. (4) and (6)].

The peak thermal load at the center of the photon beam at the monochromator, was 29 W/mm^2 for normal incidence with 70 mA of beam in the storage ring at 5.4 GeV. A plot of the peak temperature of the thermal bump verses flow rate of the liquid gallium for different synchrotron beam currents is given in Fig. 9. At first, the peak temperatures drop rapidly as the flow changes from laminar to turbulent and the distribution of the flow in the channels becomes more uniform. In this region Eq. (9) is not a good approximation

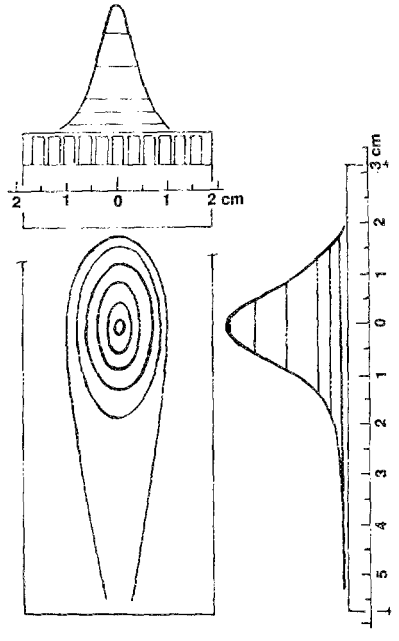

FIG. 8. Thermal profile of the undulator beam superimposed on the cross section of the slotted silicon crystal with the thin top layer. The side view and front view are crossed by lines at heights that correspond to the thermal contours shown in the bottom view.

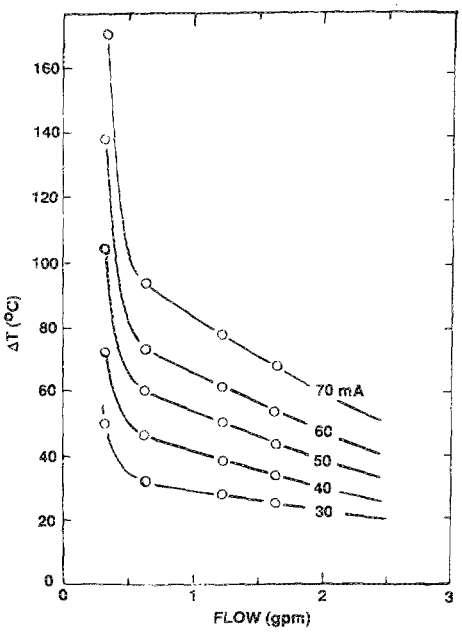

FIG. 9. Plot of the peak temperature of the thermal profile as a function of the rate of flow of the cooling fluid for the slotted crystal.

for ΔT_{23}, the temperature difference at the solid-liquid interface. This is also the region where the thermal gradients extend down into the fin structure. This gives rise to an increase in the effective value of D, and thus an increase in both the bowing and the thermal bump. Part of the strong variation in peak temperature of the thermal profile with flow rate comes from these effects. For flow rates of 0.6 gpm and above, the flow pattern stabilizes and Eq. (9) is a good approximation for ΔT_{23}. In this region the peak of the thermal profile shows an almost linear dependence on flow rate and agrees well with the $V^{0.8}$ dependence for the value of h given in Eq. (9), which leads to a similar dependence for the peak temperature of the thermal profile. All curves in Fig. 9 are decreasing with increasing flow rates so considerable improvement can be made by further increases in the flow rate. The peak temperature will approach a constant temperature given by Eq. (3), at high flow rates. This corresponds to the temperature difference across the top layer of the crystal, ΔT_{12}. This lower limit for the 70-mA curve is about 18 °C and for the lowest curve at 30 mA is about 8 °C. Doubling the flow rate to 3.2 gpm would reduce the maximum temperature for the 70-mA curve from 68 to 43 °C and for the 30-mA curve from 25 to 16 °C.

The second gallium-cooled crystal tested was 7.7 cm wide, 7.7 cm long, and 2 cm thick, with two sets of five cooling channels, 5 mm in diam. The center line of the first set of channels was 5 mm below the surface giving a minimum distance to the surface of the crystal of 2.5 mm. The second set was 15 mm below the surface. The cross section and thermal foot print for this crystal are shown in Fig. 10. The energy of the diffracted beam is 8 keV and the incident angle about 13°. The thermal profile is narrower than it was for the slotted crystal as would be expected because the lower energy beam strikes the crystal more perpendicular to the surface. The thicker top layer of the silicon crystal and the smaller thermal footprint will generate a larger ΔT_{12}. This

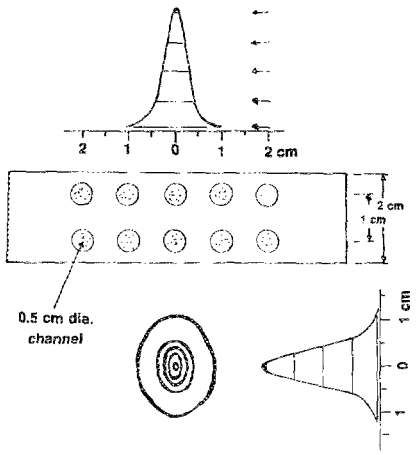

FIG. 10. Thermal profile of the undulator beam superimposed on the cross section of the 10-channel crystal. The side view and front view are crossed by lines at heights that correspond to the thermal contours shown in the bottom view.

will be reduced by some 10%–20% by the more efficient fin-cooling of the much thicker rib structure but the ΔT_{12} will still be much larger for this crystal as compared to the slotted crystal. The larger ΔT_{12} will generate larger distortions of the crystal and thus wider rocking curves. Figure 11 compares the width of the rocking curves of the two gallium-cooled crystals as a function beam current and gallium flow rate. The upper two curves are for the dual level 10-channel crystal. The upper curve is the case for 8-keV diffraction with a gallium flow of 0.62 gpm and the lower curve for 13-keV diffraction with 1.22-gpm flow. The lower slope of the second curve reflects both the larger thermal footprint and thus lower heat load per unit area of the more spread out beam of the 13-keV diffraction case and the more efficient cooling of the higher gallium flow rate. Higher flow rates will lower both of these curves. The lower four curves are for the slotted crystal with the very thin top layer, with gallium flow rates that vary from 0.26 to 1.62 gpm. Again, further improvement is possible with increased flow rates. The almost linear dependence of these curves on electron beam current makes it possible to extrapolate these curves to high-

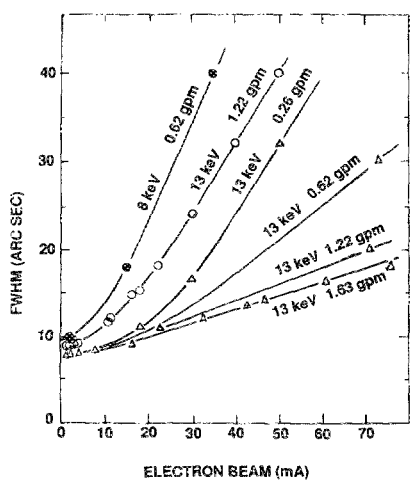

FIG. 11. Plot of the FWHM of the rocking curves of the ten-channel crystal (circles) and the slotted crystal (triangles) for different diffraction energies and flow rates for the cooling fluid (Ga), as a function of the electron beam current in the storage ring.

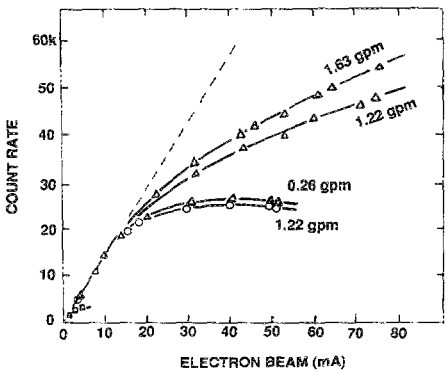

FIG. 12. Plot of the counting rate in the photon beam from the monochromator vs the electron beam current, for the slotted crystal (triangles), the ten-channel crystal (circles) and the standard CHESS side-cooled crystal (squares), with different flow rates for the cooling fluid.

er beam currents that will be available in the future. The curves for the 10-channel crystal start out higher than those for the slotted crystal. This is a result of the slightly mosaic structure of the virgin material from which the 10-channel crystal was fabricated.

Figure 12 is a plot of the count rate of the photon beam after it is diffracted by the second crystal in the two crystal monochromator as a function of the electron beam current in the synchrotron storage ring and gallium flow rate. If there were no distortion in the diffraction crystals these curves would be straight lines (see dashed curve). Again we see considerable improvement with increased gallium flow and the better results for the slotted crystal with its much thinner top layer. It is interesting to note that at low flow rates, 0.26 gpm, the performance of the slotted crystal is very similar to the high flow case of the 10-hole crystal with its much thicker top layer. This is believed to be due to the poorer heat transfer in the slotted crystal at low flow rates that come from the poorer flow pattern, less flow at the ends of the narrow slots. This poorer cooling of the fins, extends the thermal gradient down into the fin structure and increases the effective thickness of the top layer, D. The height of the thermal bump is proportional to the square of the thickness of the top layer, so modest penetrations of the thermal gradient into the fin structure will generate large changes in the height of this distortion. This is the same effect that one sees in dependence of the peak values for the thermal profile on flow rate in Fig. 9.

No matter how high the value of h is made through good cooling of the silicon crystal there will always be some bowing of the crystal and some height to the thermal bump unless an active way is found to correct the shape of the surface. The ten-channel crystal with its two levels of cooling channels is designed to accomplish this type of active control of the diffraction surface of the crystal.[7] By raising the temperature of the cooling fluid in the lower channels above that flowing in the upper channels, one can make the upper surface concave and actively compensate for the bowing and for the thermal bump. This effect was demonstrated with the ten-channel crystal during the ANL/CHESS undulator run.[7]

Although considerable progress has been made and much has been learned about the art of cooling silicon crystals with liquid metals, much more needs to be done before the next generation of synchrotrons comes on line. Further experiments need to be performed to see just how thin the top layer of the crystal can be made before the crystalline planes become distorted and to demonstrate how much improvement is possible with increased flow of the cooling fluid. Experiments with the two levels of cooling channels will also be most interesting. The latest version of this experiment uses film resistors on the back surface of the crystal to apply heat to the back of the crystal in place of the second level of cooling channels. This opens up the possibility of much greater control of the diffraction surface of the crystal than can be obtained with the two sets of cooling channels.

ACKNOWLEDGMENTS

The authors wish to thank J. Viccaro and D. Mills of ANL for many helpful discussions. This work was supported by the U.S. Department of Energy, BES-Materials Science, under Contract No. W-31-109-ENG-38.

[1] R. K. Smither, G. A. Forster, C. A. Kot, and T. M. Kuzay, Nucl. Instrum. Methods A **266**, 517 (1988).
[2] W. R. Edwards, E. H. Hoyer, and A. C. Thompson, Proc. Soc. Photo-Opt. Instrum. Eng. **582**, 281 (1985).
[3] W. M. Rohsenow and H. Y. Choi, *Heat, Mass, and Momentum Transfer* (Prentice-Hall, Englewood Cliffs, NJ, 1961), Chaps. 5–11; A. J. Chapman, *Heat Transfer* (Macmillan, New York, 1974), Chaps. 5–13.
[4] B. Batterman, D. Bilderback, C. Henderson, E. Blum, J. Vicaro, S. Kim, D. Mills, G. Shenoy, K. Robinson, F. James, S. Slater, these proceedings.
[5] D. Bilderback, C. Henderson, J. White, R. K. Smither, and G. A. Forster, these proceedings.
[6] D. Bilderback, these proceedings.
[7] R. Smither, these proceedings.